PHILOSOPHICAL MAGAZINE, 2003, VOL. 83, NO. 2, 165–178

Synthesis and characterization of mixed-valence barium titanates

THOMAS HÖCHE†, PAULA OLHE, RALF KEDING, CHRISTIAN RÜSSEL‡

Otto-Schott-Institut, Friedrich-Schiller-Universität
Fraunhoferstrasse 6, D-07743 Jena, Germany

PETER A. VAN AKEN

Institut für Angewandte Geowissenschaften, Technische Universität Darmstadt, Schnittspahnstraße 9, D-64287 Darmstadt, Germany

REINHARD SCHNEIDER‖

Lehrstuhl für Kristallographie, Institut für Physik, Humboldt-Universiät zu Berlin, Invalidenstrasse 110, D-10115 Berlin, Germany

HANS-JOACHIM KLEEBE¶

Metallurgical and Materials Engineering Department, Colorado School of Mines, Golden, Colorado 80401, USA

XIQU WANG††, ALLAN J. JACOBSON

Department of Chemistry, University of Houston, Houston, Texas 77204-5641, USA

and SUSANNE STEMMER‡‡

Materials Department, University of California, Santa Barbara, California 93106, USA

[*Received 9 October 2001 and accepted in revised form 9 August 2002*]

ABSTRACT

A single-crystal barium oxotitanate(III, IV) of approximate composition $Ba_{5.93}(Ti^{3+}_{11.86}Ti^{4+}_{28.14})O_{80}$, containing mixed-valence Ti, was grown from a borate flux. The crystal structure was identified as hollandite type by single-crystal X-ray diffractometry. Electron-energy-loss spectroscopy of Ti $L_{2,3}$ and O K edges was used to determine chemical shifts related to the presence of mixed-valence Ti in the crystal. Comparison of Ti $L_{2,3}$ and O K energy-loss near-edge structure

† Present address: Institut für Oberflächenmodifizierung e.V., Permoserstrasse 15, D-04318 Leipzig, Germany. E-mail: hoeche@uni-leipzig.de.
‡ Email: ccr@r2.uni-jena.de.
§ Email: vanaken@geo.tu-darmstadt.de.
‖ Email: reinhard.schneider@physik.hu-berlin.de.
¶ Email: hkleebe@mines.edu.
†† Email: wangx@bayou.uh.edu.
‡‡ Email: stemmer@mrl.ucsb.edu.

Philosophical Magazine ISSN 1478–6435 print/ISSN 1478–6443 online © 2003 Taylor & Francis Ltd
http://www.tandf.co.uk/journals
DOI: 10.1080/0141861021000028367

(ELNES) of $Ba_{5.93}(Ti^{3+}_{11.86}Ti^{4+}_{28.14})O_{80}$ with those obtained from a $K_{1.54}Mg_{0.77}Ti_{7.23}O_{16}$ single crystal with hollandite structure, containing only Ti^{4+}, revealed a shift in the Ti $L_{2,3}$ edge by 0.4–0.5 eV towards lower energy losses whereas only slight intensity variations without a detectable energy shift of the edge onset occur at the O K ELNES. In addition, valence-specific multiplet structures of the Ti L_{23} ELNES are used as valence fingerprints. The observed fine structures of O K and Ti $L_{2,3}$ edges can be used to interpret coordination and bonding in related compounds.

§ 1. Introduction

Barium titanate ($BaTiO_3$) is an important electroceramic because of its excellent ferroelectric properties and high dielectric permittivity. A number of technologically important properties of this material are determined by valence state changes of Ti, often controlled by doping (Aggarwal and Ramesh 1998). The spatial distribution of Ti with different valence states within the microstructure, for example at grain boundaries, also determines the electrical behaviour of barium titanates.

A method suitable for spatially resolved analysis of point defects is electron-energy-loss spectroscopy (EELS) in transmission electron microscopy (TEM) (Egerton 1996). Changes in bonding, coordination and ionic charge, as associated with materials defects, are reflected in the intensity distribution of the energy-loss near-edge fine structure (ELNES) of core loss edges. In practice, ELNES is often interpreted by comparing features in the ELNES of the defect with features of compounds with known valence states and coordination of a particular atom ('fingerprinting'), as a comprehensive theoretical framework for ELNES interpretation is still being developed.

The structure of $BaTiO_3$ is based on that of perovskite, in which Ti is coordinated octahedrally with O. In stoichiometric $BaTiO_3$, Ti is present in a formal valence state of 4+. The goal of the present work is the synthesis of barium titanates which contain Ti in octahedral coordination with O in a mixed-valence state to provide an improved understanding of changes of the ELNES with Ti valence state in $BaTiO_3$ and related compounds.

Several groups (Brydson *et al.* 1989, 1992, 1993, de Groot *et al.* 1992, Crocombette and Jollet 1994, Ruus *et al.* 1997, Yoshiya *et al.* 1999) have demonstrated that Ti $L_{2,3}$ ELNES can be used to identify various Ti(IV)–O compounds. Schneider *et al.* (1996) and Abicht *et al.* (1997) were able to discern phases in multiphase ceramics on the basis of Ti $L_{2,3}$ and O K ionization edges. ELNES from mixed-valence Ba–Ti–O compounds has not yet been reported.

In the literature, barium titanates containing mixed-valence Ti, or barium oxotitanates(III, IV), have been reported with compositions $Ba_2Ti_6O_{13}$ (Schmachtel and Müller-Buschbaum 1977), $Ba_2Ti_{13}O_{22}$ (Möhr and Müller-Buschbaum 1993, Akimoto *et al.* 1994), and $Ba_xTi_8O_{16}$ (with x between 1.07 and 1.31) (Cheary and Squadrito 1989, Cheary *et al.* 1996). Höche *et al.* (2001) reported needles containing only Ti^{3+} (approximate formula; $BaTi_6O_{10}$) formed in a BaO–TiO_2–Ti_2O_3–SiO_2 melt. $BaTi_8O_{16}$ was found to crystallize in the hollandite structure (Schmachtel and Müller-Buschbaum 1980). Cheary (1990) reported structural changes (the amount of monoclinic distortion) of a hollandite $Ba_xTi^{3+}_{2x}Ti^{4+}_{8-2x}O_{16}$ (with x between 1.07 and 1.31) in the temperature range between 5 and 500 K.

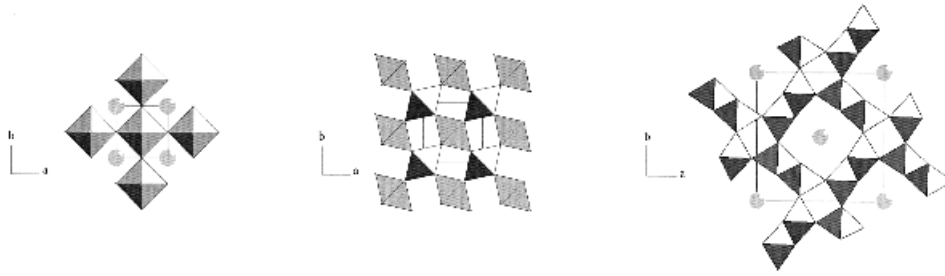

Figure 1. Graphic representation of the crystal structures of (*a*) perovskite ($BaTiO_3$), (*b*) hollandite ($K_{1.54}Mg_{0.77}Ti_{7.23}O_{16}$) and (*c*) rutile ($TiO_2$). Note the differently connected TiO_6 octahedra in the three structures.

Here we report a method for the synthesis and EELS of a single-crystal, mixed-valence barium oxotitanate(III, IV). The synthesis method described here is of technological interest to produce controlled-valence state materials with potentially interesting properties. The ELNES of the mixed-valence barium oxotitanate(II, IV) will be interpreted using isostructural hollandite containing only Ti^{4+}, perovskite $BaTiO_3$ and rutile TiO_2 for comparison. The crystal structures of the compounds, all consisting of (slightly distorted) TiO_6 octahedra, are depicted in figure 1.

§ 2. Experimental details

2.1. *Single-crystal growth and reference materials*

The starting material, Ba_2TiO_4, was synthesized by calcining $BaCO_3$ and TiO_2 powders first at 1200°C for 2 h and then, after regrinding, at 1500°C for 16 h. Ba_2TiO_4 and a second starting material, Ti_2O_3, were intimately mixed by collective grinding. Pellets were obtained by uniaxial pressing and fired at 1200°C for 16 h under inert conditions (Ar atmosphere) in order to produce $Ba_2Ti_{13}O_{22}$:

$$Ba_2TiO_4 + 6Ti_2O_3 \rightarrow Ba_2Ti_{13}O_{22}. \quad (1)$$

Black pellets of the reaction product were reground and blended with $BaO \cdot 2B_2O_3$ flux in a weight ratio of 1 : 2. About 5 g of the mixture were enclosed in Mo foil and heat treated under flowing H_2. After soaking for 24 h at 1300°C, the sample was first slowly (10 K h^{-1}) cooled down to 650°C and then rapidly to room temperature. During this procedure, most of the flux evaporated, leaving needle-shaped crystals jutting out of the sediment. These needles were not wetted with flux residual and were used for further examination.

The $K_{1.54}Mg_{0.77}Ti_{7.23}O_{16}$ hollandite single crystals used as a reference were also grown from high-temperature solutions as described by Beyeler and Schlüter (1980). The other reference compound, $BaTiO_3$, was synthesized by finely grinding and intimately mixing appropriate amounts of reagent-grade $BaCO_3$ and TiO_2 followed by a heat treatment at 1200°C for 2 h.

2.2. *Crystal structure determination*

Single crystal X-ray data of selected crystals were recorded using a four-circle single-crystal diffractometer (SMART platform) and graphite-monochromated Mo

Kα radiation at room temperature. For each phase, a hemisphere of data (1271 frames at a 5 cm detector distance) was collected using a narrow-frame method with scan widths of 0.30° in ω and an exposure time of 30 s frame^{-1}. The first 50 frames were remeasured at the end of data collection to monitor the instrument and crystal stability, and the maximum correction applied to the intensities was less than 1%. The data were integrated using the Siemens SAINT program, with the intensities corrected for Lorentz factor, polarization, air absorption and absorption due to variation in the path length through the detector faceplate. Following absorption correction (using the computer code SADABS), the structure was solved by direct methods and refined anisotropically (using SHELXTL). For $K_{1.54}Mg_{0.77}Ti_{7.23}O_{16}$, the lattice parameters reported by Weber and Schulz (1983) and Rosshirt *et al.* (1990, 1991), were reproduced within a few parts per million using the same diffractometer and data analysis technique.

2.3. *Scanning electron microscopy and transmission electron microscopy investigation*

The barium oxotitanate(III, IV) needles were examined by scanning electron microscopy (Zeiss DSM 940A) equipped with an energy-dispersive X-ray spectrometer (Oxford Instruments eXL10) and a wavelength-dispersive X-ray analyser (Microspec 3PC). Crystals of barium oxotitanate(III, IV) and $K_{1.54}Mg_{0.77}Ti_{7.23}O_{16}$ respectively were crushed and placed on lacey-C-film-coated Cu grids for examination in the transmission electron microscope.

Selected-area electron diffraction patterns were recorded using a Hitachi H-8100 II transmission electron microscope operated at 200 kV. EELS was performed using a Philips CM12 transmission electron microscope operated at 120 kV with an undersaturated LaB_6 cathode and a Gatan DigiPEELS 766. Energy resolution, defined as the full width ΔE_{FWHM} at half-maximum of the zero-loss peak, was determined as $\Delta E_{FWHM} = 0.7$ eV. Experimental methods and evaluation of EELS data have been described by van Aken and Liebscher (2002) and include corrections for dark current and noise as well as for channel-to-channel gain variations of the detector. The background was subtracted using an inverse power-law function. Multiple scattering and tailing effects of the zero-loss peak were deconvoluted by the Fourier ratio technique (Egerton 1996) using the corresponding low-loss spectra, acquired consecutively to core-loss edges from the same specimen region. For energy calibration, the Ba M5 white-line maximum in each spectrum was placed at 784.7 eV (Guerlin 1996). Ba is assumed to be divalent in all compounds studied here (Cohen and Krakauer 1990). We therefore expect the energy position of the Ba $M_{4,5}$ edges to be insensitive to changes in the Ti valence state and coordination, and thus suitable for energy calibration. The π* peak maximum at 285.05 eV in the C K ELNES of the lacey-C film was used as a second internal energy reference. For energy calibration, the C K, Ti $L_{2,3}$, O K and Ba $M_{4,5}$ edges were recorded first at an energy dispersion of 0.5 eV channel^{-1}. Subchannel resolution of the peak positions with an estimated accuracy of ±0.2 eV was achieved by post-acquisition interpolation. Next, the Ti L_{23} and O K edges were measured at 0.1 eV channel^{-1} dispersion in order to resolve distinct spectral features. For $K_{1.54}Mg_{0.77}Ti_{7.23}O_{16}$ and for rutile TiO_2, the calibration of the electron-energy-loss spectra was performed using the C K ELNES π* peak only.

§ 3. Results and discussion

All results were obtained from barium oxotitanate(III, IV) crystals with well-developed facets grown by the flux technique. X-ray single-crystal diffractometry revealed that some crystals were of insufficient quality for reliable single-crystal structure analysis owing to crystal defects, which included twinning and intergrowth. A scanning electron micrograph of a flux-grown needle-shaped crystal is shown in figure 2. This crystal was 500 μm long and about 30 μm in diameter with an almost hexagonal cross-section. It was black coloured and consisted of well-developed facets perpendicular to its needle axis. This crystal was selected for single-crystal structure determination and EELS.

The composition of this crystal was determined by X-ray diffractometry (described below) to be $Ba_{1.19}Ti^{3+}_{2.38}Ti^{4+}_{5.62}O_{16}$ and, within the detection limits, this composition was reproduced by energy-dispersive X-ray spectroscopy using a Co standard. No B from the borate flux was detected by wavelength-dispersive X-ray spectroscopy in the crystal. The structural characterization of $K_{1.54}Mg_{0.77}Ti_{7.23}O_{16}$

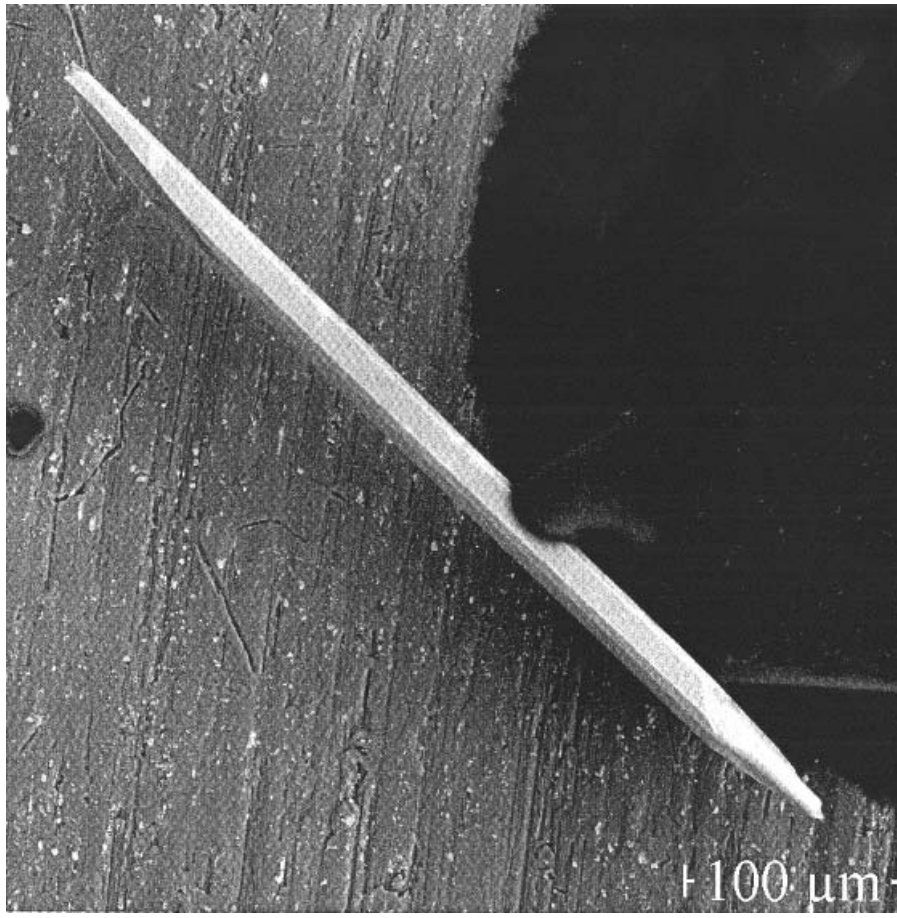

Figure 2. Scanning electron micrograph of the $Ba_{1.2}Ti_8O_{16}$ needle analysed by four-circle diffractometry before crushing to prepare the TEM sample (micrometre-sized slivers on a lacey-C-film coated Cu grid).

crystals was reported earlier by Weber and Schulz (1983) and $K_{1.54}Mg_{0.77}Ti_{7.23}O_{16}$ was found to possess a hollandite structure.

3.1. *Crystal structure determination*

A monoclinic body-centred unit cell with cell dimensions $a = 9.994\,2(9)$ Å, $b = 14.785(1)$ Å, $c = 10.266(1)$ Å and $\beta = 90.88(1)^\circ$ (non-standard orientation) was derived from the single-crystal diffraction data (table 1). The R factor was 0.055. The crystal structure was successfully solved and refined in the space group $I2/m$ (No. 12) and is depicted in figure 3. It is very similar to that of $BaTi_8O_{16}$ hollandite (Schmachtel and Müller-Buschbaum 1980). Together with the compositional data, the needle was identified as $Ba_{5.93}Ti_{40}O_{80}$ (or $Ba_{1.19}Ti^{3+}_{2.38}Ti^{4+}_{5.62}O_{16}$).

In this crystal, six symmetry-independent Ti positions (table 2), each coordinated to six O atoms, form distorted octahedra with Ti—O bond lengths of about 1.901–2.041 Å. These octahedra share edges to form double chains along [010]. The double chains are linked via sharing octahedral corners and form a framework that contains open 1×1 and 2×2 channels running along [010]. Disordered Ba cations are located in the 2×2 channels. Bond valence sums calculated for the Ti sites using the bond valence parameter for Ti(IV)–O bonds are in the range of 3.77–3.93 vu, which may indicate that there is no charge ordering. A fivefold superstructure along the Ba-bearing channels formed by TiO_6 octahedra (the crystallographic b direction) is observed in $Ba_{1.19}Ti^{3+}_{2.38}Ti^{4+}_{5.62}O_{16}$, although not found in the basic hollandite structure. This superstructure can be considered as a commensurate form of a compound structure (Perez-Mato *et al.* 2001). Such commensurate superstructures along the large-cation tunnel direction have been observed in $(Ba_{1.14}K_{0.05})(Ti_{5.81}V_{1.34}Cr_{0.36}Fe_{0.20}Mn_{0.16}Al_{0.09})(OH)_{16}$ (Bolotina *et al.* 1992), $Ba_{1.33}Ti_{6.67}Mg_{1.33}O_{16}$ (Bursill and Grzinic 1980), and $Ba_{1.2}Ti_{6.8}Mg_{1.2}O_{16}$ (Bursill and Grzinic 1980, Fanchon *et al.* 1987).

It is interesting to note that the previously reported $Ba_{1.2}Ti_{6.8}Mg_{1.2}O_{16}$ (space group, $I2/m, a = 10.227(3)$ Å; $b = 14.907(8)$ Å; $c = 9.964(6)$Å; $\beta = 90.77(4)^\circ$) (Fanchon *et al.* 1987) possesses a crystal structure very similar to that of the $Ba_{1.19}Ti_8O_{16}$ observed here. Although the lattice constants a and b of $Ba_{1.2}Ti_{6.8}Mg_{1.2}O_{16}$ are significantly larger than those of $Ba_{1.19}Ti_8O_{16}$ (the ionic radius of Mg^{2+} in octahedral coordination is about 15% larger than that of identically coordinated Ti^{4+}) and c is smaller (presumably because of preferential ordering of Mg^{2+} among Ti^{4+} sites (Cheary and Squadrito 1989)), the monoclinic angle β is almost identical.

Table 1. Crystallographic data.

Formula sum	$Ba_{5.93}Ti_{40}O_{80}$ $(= 5Ba_{1.19}Ti^{3+}_{2.38}Ti^{4+}_{5.62}O_{16})$
Crystal system	Monoclinic
Space group	$I12/m1$ (No. 12)
Unit-cell dimensions	$a = 9.994\,2(9)$ Å
	$b = 14.785\,1(14)$ Å
	$c = 10.265\,5(10)$ Å
	$\beta = 90.88(1)^\circ$
Cell volume	1516.70(25) Å
R factor	0.055

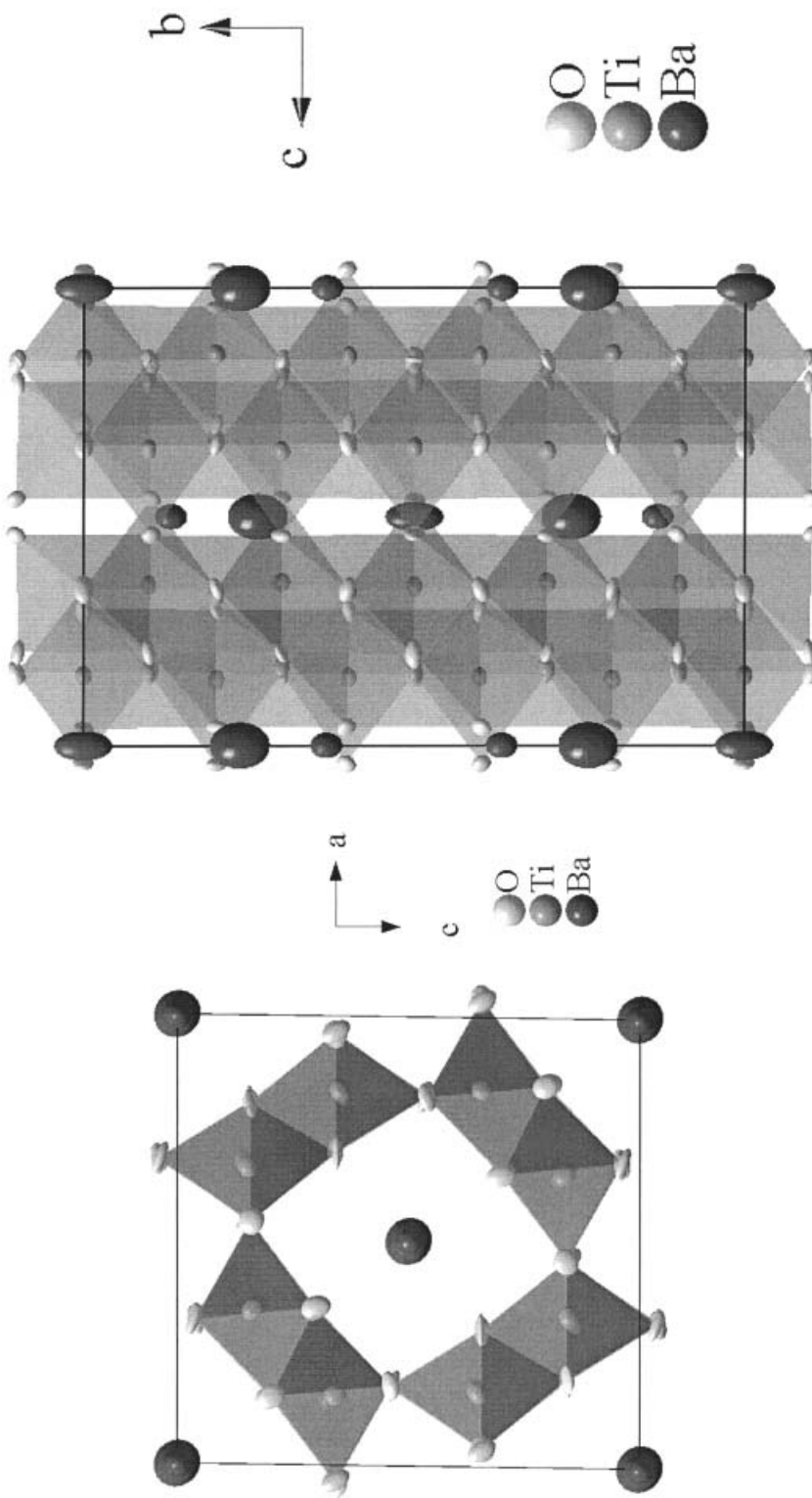

Figure 3. Graphic representation of the structural model derived from X-ray diffraction data projected along the crystallographic *b* and *a* axes.

Table 2. Atomic coordinates of $Ba_{5.93}Ti_{40}O_{80}$.

Atom	Wyckhoff site	Occupancy	*x*	*y*	*z*
Ba(1a)	4g	0.5	0	0.367 70	0
Ba(1b)	4g	1	0	0.237 00	0
Ba(2)	2a	0.242	0.5	0.5	0.5
Ti(1)	8j	1	0.333 31	0.401 37	−0.148 33
Ti(2)	4i	0.5	0.162 92	0.5	−0.347 51
Ti(3)	8j	1	0.174 09	0.299 43	−0.356 41
Ti(4)	8j	1	0.153 05	0.401 65	0.336 66
Ti(5)	8j	1	0.147 92	0.200 58	0.329 97
Ti(6)	4i	0.5	−0.342 10	0.5	−0.159 18
O(1)	8j	1	0.320 74	0.397 86	0.039 46
O(2)	8j	1	0.041 61	0.201 00	−0.343 03
O(3)	8j	1	0.196 87	0.300 08	−0.158 48
O(4)	4i	0.5	0.193 85	0.5	−0.155 84
O(5)	4i	0.5	0.179 62	0.5	−0.536 46
O(6)	8j	1	0.040 02	0.399 03	−0.340 73
O(7)	8j	1	0.697 36	0.598 76	−0.658 08
O(8)	8j	1	0.152 31	0.299 05	0.203 57
O(9)	8j	1	0.326 01	0.201 09	0.041 64
O(10)	8j	1	−0.347 51	0.598 49	−0.295 45
O(11)	4i	0.5	0.148 91	0.5	0.200 03
O(12)	4i	0.5	−0.535 72	0.5	−0.157 81

EELS indicated that minor concentrations of Ca (a few mole per cent) might have been incorporated into the $Ba_{1.19}Ti^{3+}_{2.38}Ti^{4+}_{5.62}O_{16}$ lattice. Ca is unlikely to occupy octahedral Ti sites, and the possible substitution of Ca for Ba was considered in the structure refinement. About 5% Ba(2) (or 1.7% total Ba) can be replaced by Ca without substantially lowering the refinement accuracy ($R = 0.0558$). The influence of Ca on Ba sites on the Ti $L_{2,3}$ ELNES and O K ELNES is expected to be very minor, for reasons explained below. The structural quality of the $Ba_{1.19}Ti_8O_{16}$ hollandite crystal was checked by high-resolution TEM in order to assure the

Table 3. Ti—O bond length of $Ba_{5.93}(Ti^{3+}_{11.86}Ti^{4+}_{28.14})O_{80}$ and $K_{1.54}Mg_{0.77}Ti_{7.23}O_{16}$.

	Bond length (Å) for the following crystallographic sites					
Compound	Ti(1)	Ti(2)	Ti(3)	Ti(4)	Ti(5)	Ti(6)
$Ba_{5.93}(Ti^{3+}_{11.86}Ti^{4+}_{28.14})O_{80}$	1.935	1.935	1.901	1.931	1.901	1.935
	1.963	1.935	1.961	1.967	1.951	1.956
	1.966	1.950	1.974	1.976	1.977	1.956
	2.006	1.987	1.982	1.995	1.984	1.982
	2.018	2.021	1.999	2.021	2.000	2.019
	2.027	2.021	2.041	2.041	2.031	2.019
$K_{1.54}Mg_{0.77}Ti_{7.23}O_{16}$	1.926					
	1.972					
	1.972					
	1.974					
	1.974					
	2.020					

absence of defects such as twins. Besides very weak lines of diffuse intensity†, no higher-dimensional defects were apparently observable in electron diffraction patterns. The hollandite $K_{1.54}Mg_{0.77}Ti_{7.23}O_{16}$ used as reference material showed Ti—O bond lengths and angles similar to $Ba_{1.19}Ti_8O_{16}$ (table 3).

3.2. *Electron energy-loss near-edge structures*

Figures 4(*a*) and (*b*) shows Ti $L_{2,3}$ and O K energy-loss near-edge structures respectively for $Ba_{1.19}Ti_8O_{16}$, $K_{1.54}Mg_{0.77}Ti_{7.23}O_{16}$, $BaTiO_3$ and TiO_2 (rutile) after energy calibration as described in § 2.3. While the latter three samples nominally posses a d^0 configuration, in $Ba_{1.19}Ti^{3+}_{2.38}Ti^{4+}_{5.62}O_{16}$ some d^1 character is blended in owing to the partial reduction of Ti^{4+} towards Ti^{3+}.

The fine-structure of Ti $L_{2,3}$ edges reflects dipole-allowed transitions of inner-shell Ti 2p electrons to the relatively narrow unoccupied 3d band, of predominantly Ti 3d character hybridized with a significant amount of O 2p character (Leapman *et al.* 1982). The Ti 2p core–hole spin–orbit interaction splits the spectrum into two parts, resulting in Ti L_3 and Ti L_2 white lines with a separation of about 5.4 eV which are further split by low-symmetry ligand field. For octahedral coordination of Ti with O, the Ti L_3 and Ti L_2 edges are split because of the crystal-field splitting of the excited 3d orbitals into low-energy t_{2g} and high-energy e_g orbitals (Leapman *et al.* 1982). According to Fink *et al.* (1985), lifetime broadening of transition-metal 2p levels is approximately 0.2 eV for Ti. The ELNES facilitates the discrimination

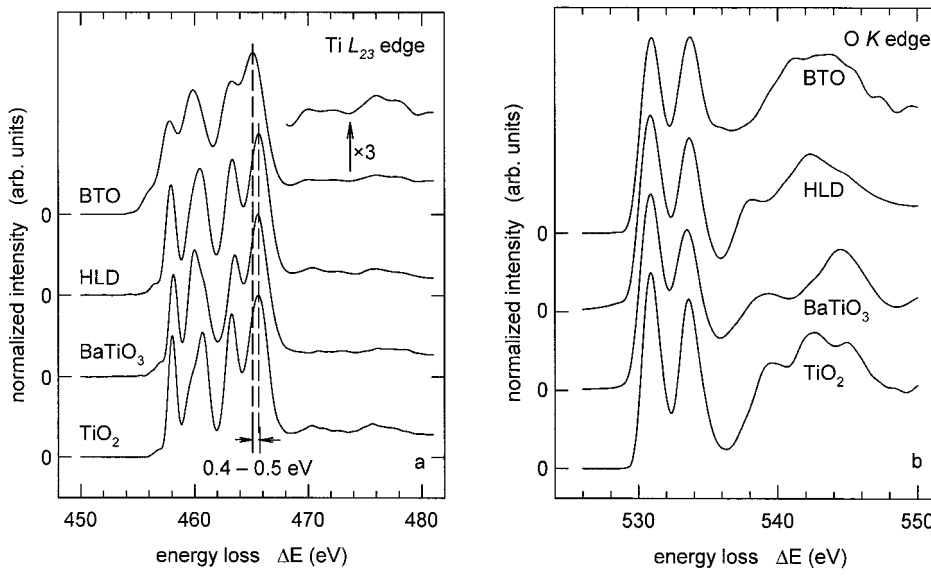

Figure 4. (*a*) Ti-$L_{2,3}$ and (*b*) O K ELNESs of $Ba_{1.19}Ti^{3+}_{2.38}Ti^{4+}_{5.62}O_{16}$ (BTO), $K_{1.54}Mg_{0.77}Ti_{7.23}O_{16}$ (HLD), $BaTiO_3$ and rutile TiO_2.

† Ordering phenomena responsible for diffusely scattered intensities have been addressed by Fanchon *et al.* (1987). Their influence on electron-energy-loss spectra is very minor so that they are not further considered.

of minor differences provoked by the presence of Ti of valence 3+. The Ti $L_{2,3}$ edge reflects the nearest-neighbour environment (Brydson *et al.* 1989, de Groot *et al.* 1992, Crocombette and Jollet 1994), which is similar in all materials investigated here (octahedral coordination of Ti with O). The Ti L_3 e_g peaks of $K_{1.54}Mg_{0.77}Ti_{7.23}O_{16}$, $BaTiO_3$ and TiO_2 at around 461 eV (figure 4 (*a*)) exhibit a double-peak structure with characteristic intensity ratios. Similar observations have been made for the different TiO_2 polymorphs rutile, anatase and brookite (Brydson *et al.* 1989, Crocombette and Jollet 1994, Ruus *et al.* 1997). Within the energy resolution available, no further significant differences in the fine structure of the Ti $L_{2,3}$ edges are therefore expected unless Ti is present at a reduced valence. For $Ba_{1.19}Ti^{3+}_{2.38}Ti^{4+}_{5.62}O_{16}$, the crystal-field splitting of the Ti $L_{2,3}$ ELNES (figure 4 (*a*)) seems to be smaller, since t_{2g} and e_g features are less clearly separated and appear to be broader, although the energy resolutions of the TEM–EELS system were the same for all spectra presented. Higuchi *et al.* (1999) assigned spectral features at 471 and 476 eV in X-ray absorption spectra of $La_xSr_{1-x}TiO_3$ to charge-transfer transitions between occupied O 2p bands and unoccupied Ti 3d states. Corresponding peaks are also found in Ti $L_{2,3}$ spectra of $Ba_{1.19}Ti^{3+}_{2.38}Ti^{4+}_{5.62}O_{16}$, $K_{1.54}Mg_{0.77}Ti_{7.23}O_{16}$, $BaTiO_3$ and TiO_2. For $Ba_{1.19}Ti^{3+}_{2.38}Ti^{4+}_{5.62}O_{16}$, onset energies of about 470 and 475 eV are found as illustrated by the intensity-enhanced inset in figure 4 (*a*).

The crystal-field splitting is also reflected in the O K edge features (figure 4 (*b*)) (Brydson *et al.* 1989). Note the two strong t_{2g} and e_g features for $K_{1.54}Mg_{0.77}Ti_{7.23}O_{16}$ and TiO_2, where t_{2g} is slightly more intense than e_g. In the perovskite $BaTiO_3$, the intensity ratio of e_g to t_{2g} is slightly further shifted towards t_{2g}. This intensity difference is thought to fingerprint the threefold planar coordination of O with Ti in rutile versus a linear twofold coordination in perovskite (Brydson *et al.* 1989). The similarity in the relative intensities of peaks t_{2g} to e_g in rutile and hollandite supports this interpretation. In the O K spectrum of $Ba_{1.19}Ti^{3+}_{2.38}Ti^{4+}_{5.62}O_{16}$, the e_g peak slightly surmounts the t_{2g} peak. Following the above interpretation, this discrepancy is thought to be caused by the distortion of coordination polyhedra in $Ba_{1.19}Ti^{3+}_{2.38}Ti^{4+}_{5.62}O_{16}$ in comparison with $K_{1.54}Mg_{0.77}Ti_{7.23}O_{16}$ (table 3).

Broadened features at higher energy losses between 536 and 548 eV involve transitions to O 2p states hybridized with transition-metal 4s and 4p states. Since features in this region are believed to reflect the (O) second-nearest-neighbour environment (Brydson *et al.* 1992), significantly distinct features in the fine structures are observed for $BaTiO_3$, TiO_2, and the hollandites.

The Ti L_2 e_g peak maximum of the $Ba_{5.93}(Ti^{3+}_{11.86}Ti^{4+}_{28.14})O_{80}$ hollandite, containing Ti in a reduced valence state (average titanium valence, 3.7), is shifted by 0.4–0.5 eV towards lower energy losses with respect to corresponding features in the other, nominally tetravalent compounds. No energy shifts of the O K edges (using the energy loss of feature t_{2g}) could be discerned within the experimental energy resolution. Changes in the valence state shift the core level binding energies and produce shifts in edge onsets in EELS. Chemical shifts of the Ti L_{23} edges towards *lower* energy losses have been observed for Ti with lower valence (Leapman *et al.* 1982, Otten *et al.* 1985), and smaller shifts (less than 1 eV) of O K edges towards *higher* energy losses (Lusvardi *et al.* 1998, Yoshiya *et al.* 1999) have been reported, too.

In Ti-bearing mixed-valence compounds, a decomposition of the Ti 2p core levels into two components has been reported for $Y_{1-x}Ca_xTiO_3$ (Morikawa *et al.* 1996)

and $La_{1-x}Sr_xTiO_3$ (Abbate *et al.* 1991). The peak intensity attributed to Ti^{4+} (at higher energy losses) and Ti^{3+} (at lower energy losses) components was found to vary systematically (linearly) with x; that is, the relative intensities of the contributing components almost correctly reflect the d-electron concentration in the ground state (Morikawa *et al.* 1996). Besides $La_{1-x}Sr_xTiO_3$, other controlled valence materials such as $Li_xNi_{1-x}O$ have been investigated in order to determine the crystallographic site where the additional electrons reside (Abbate *et al.* 1991). X-ray absorption spectra of $La_{1-x}Sr_xTiO_3$ could be interpreted such that with decreasing x, Ti 3d states become increasingly occupied.

In $Ba_{1.19}Ti^{3+}_{2.38}Ti^{4+}_{5.62}O_{16}$, a representative of the $Ba_xTi^{3+}_{2x}Ti^{4+}_{8-2x}O_{16}$ family (with x between 1.07 and 1.31 (Cheary 1990)), the substitution of Ti^{4+} by Ti^{3+} is charge balanced by incorporating a lower number of Ba cations into the open channels of the hollandite crystal lattice. Therefore, in comparison with hollandite structures

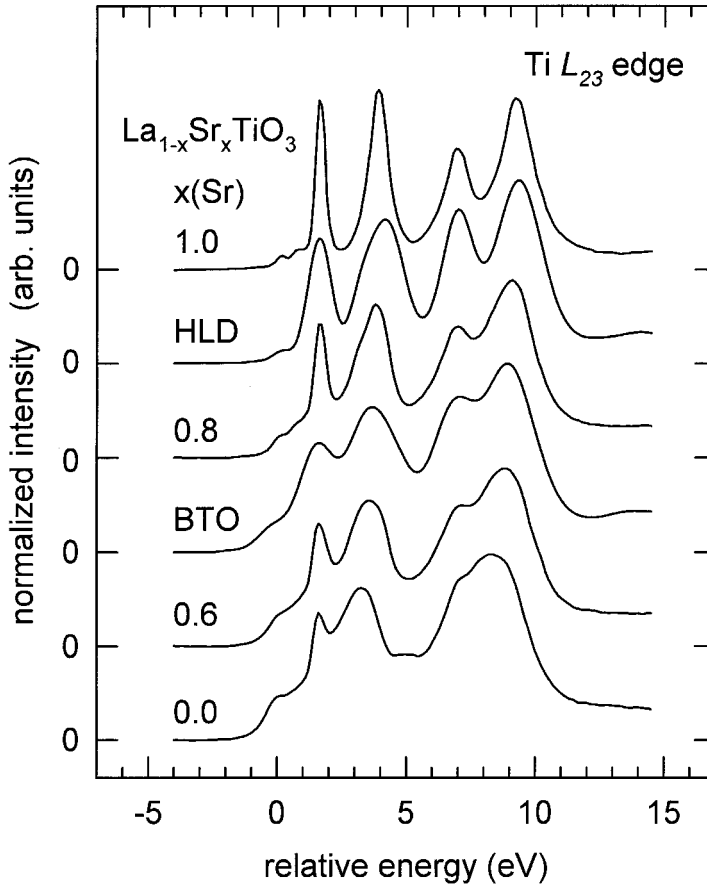

Figure 5. Ti $L_{2,3}$ ELNES of $La_{1-x}Sr_xTiO_3$ ($x = 0.0, 0.6, 0.8$ and 1.0) (data extracted from the paper by Abbate *et al.* (1991)), $Ba_{1.19}Ti^{3+}_{2.38}Ti^{4+}_{5.62}O_{16}$ (BTO) and $K_{1.54}Mg_{0.77}Ti_{7.23}O_{16}$ (HLD), plotted on a relative energy scale. The Ti L_2 e_g maximum of $K_{1.54}Mg_{0.77}Ti_{7.23}O_{16}$ has been aligned with the respective maximum for $SrTiO_3$. The energy difference of 0.4–0.5 eV between the Ti L_2 e_g maxima of $Ba_{1.19}Ti^{3+}_{2.38}Ti^{4+}_{5.62}O_{16}$ and $K_{1.54}Mg_{0.77}Ti_{7.23}O_{16}$, as shown in figure 4 (*a*), remains unchanged.

containing merely tetravalent Ti, Ti coordination with O is only slightly different (see table 3). In $Ba_{1.19}Ti^{3+}_{2.38}Ti^{4+}_{5.62}O_{16}$, 2.38 extra electrons per formula unit ($[Ti^{3+}]/[Ti^{3+} + Ti^{4+}] = 30\%$) should reside on Ti sites. In this case, the Ti $L_{2,3}$ ELNES consists of a superposition of a Ti^{4+} hollandite Ti $L_{2,3}$ ELNES (as recorded for $K_{1.54}Mg_{0.77}Ti_{7.23}O_{16}$) and a Ti^{3+} hollandite Ti $L_{2,3}$ ELNES. The latter should be slightly shifted with respect to the former towards lower energy losses.

Closer inspection of figure 4 (*a*) reveals exactly this superposition. When the Ti $L_{2,3}$ ELNES of $Ba_{1.19}Ti^{3+}_{2.38}Ti^{4+}_{5.62}O_{16}$ is compared with Ti $L_{2,3}$ X-ray absorption spectra of $La_{1-x}Sr_xTiO_3$ (figure 5 (Abbate *et al.* 1991)), it becomes obvious that $Ba_{1.19}Ti^{3+}_{2.38}Ti^{4+}_{5.62}O_{16}$ ($[Ti^{3+}]/[Ti^{3+} + Ti^{4+}] = 30\%$) fits between $La_{1-x}Sr_xTiO_3$ spectra for $x = 0.6$ (corresponding to $[Ti^{3+}]/[Ti^{3+} + Ti^{4+}] = 40\%$) and $x = 0.8$ ($[Ti^{3+}]/[Ti^{3+} + Ti^{4+}] = 20\%$). This finding further supports the idea that, also in the $Ba_xTi^{3+}Ti^{4+}_{8-2x}O_{16}$ hollandites (containing, in contrast with La-substituted $SrTiO_3$, only three elements), extra electrons reside at Ti sites. The 0.4–0.5 eV energy shift observed with the Ti L_2 e_g peak maximum of $Ba_{5.93}(Ti^{3+}_{11.86}Ti^{4+}_{28.14})O_{80}$ can be understood as resulting from the superposition of a Ti^{4+} hollandite Ti $L_{2,3}$ ELNES and an ELNES characteristic of Ti^{3+} in the hollandite structure.

In summary, in analogy to the determination of the $[Fe^{3+}]/[Fe^{3+} + Fe^{4+}]$ ratio from the Fe $L_{2,3}$ ELNES widely used in mineralogy (van Aken *et al.* 1998, van Aken and Liebscher 2002), the $[Ti^{3+}]/[Ti^{3+} + Ti^{4+}]$ ratio can be retrieved from the Ti $L_{2,3}$ ELNES. A necessary condition is that the Ti coordination with O remains the same in the unknown compound as in the reference materials. In contrast with the Fe $L_{2,3}$ ELNES, which is much less sensitive to changes in coordination, the Ti $L_{2,3}$ ELNESs of titanates with different coordinations (octahedral, pentahedral and tetrahedral) are significantely different (Langenhorst and van Aken 2000, Höche *et al.* 2001). Spatially resolved analysis of $[Ti^{3+}]/[Ti^{3+} + Ti^{4+}]$ ratios using TEM–EELS is expected to be further facilitated when transmission electron microscopes with monochromated electron sources become available (Rose 1999).

§ 4. Conclusions

We have used a flux method to synthesize a single-crystal hollandite type barium titanate which contains mixed-valence Ti in octahedral coordination with O. The fine-structures of the Ti $L_{2,3}$ and O K EELS edges of this crystal were compared with those of $BaTiO_3$, rutile TiO_2 and hollandite $K_{1.54}Mg_{0.77}Ti_{7.23}O_{16}$, all of which contain Ti in octahedral coordination with O and a formal 4+ valence. The Ti $L_{2,3}$ ELNES of $Ba_{1.19}Ti^{3+}_{2.38}Ti^{4+}_{5.62}O_{16}$ was interpreted as arising from two components attributed to Ti of valences 3+ and 4+. This finding proves that the Ti $L_{2,3}$ edge can be analysed in terms of the $[Ti^{3+}]/[Ti^{3+} + Ti^{4+}]$ ratio provided that the shape of the Ti $L_{2,3}$ ELNES does not change owing to deviations of coordination associated with the $Ti^{4+} \rightarrow Ti^{3+}$ substitution.

Acknowledgements

This work was funded by the National Science Foundation–Deutscher Akademischer Austauschdienst International Opportunities Program (NSF INT-9909963). P.O. gratefully acknowledges a scholarship granted by the Otto-Schott-Institut, Friedrich-Schiller-Universität Jena. We are grateful to Professor F. Frey, Ludwig-Maximilians-Universität München, for providing $K_{1.54}Mg_{0.77}Ti_{7.23}O_{16}$

single crystals. P.A.v.A. gratefully acknowledges the funding by the Deutsche Forschungsgemeinschaft (AK 26/2-1,2) for the upgrade of the Gatan PEELS 666 to the Gatan DigiPEELS 766.

References

Abbate, M., de Groot, F. M. F., Fuggle, J. C., Fujimori, A., Tokura, Y., Fujishima, Y., Strebel, O., Domke, M., Kaindl, G., van Elp, J., Thole, B. T., Sawatzky, G. A., Sacchi, M., and Tsuda, N., 1991, *Phys. Rev.* B, **44**, 5419.

Abicht, H.-P., Völtzke, D., Röder, A., Schneider, R., and Woltersdorf, J., 1997, *J. Mater. Chem.,* **7**, 487.

Aggarwal, S., and Ramesh, R., 1998, *A. Rev. Mater. Sci.,* **28**, 463.

Akimoto, J., Gotoh, Y., Sohma, M., Kawaguchi, K., and Oosawa, Y., 1994, *J. solid st. Chem.,* **113**, 384.

Beyeler, H. U., and Schlüter, C., 1980, *Solid St. Ionics,* **1**, 77.

Bolotina, N. B., Dmitrieva, M. T., and Rastsvetaeva, R. K., 1992, *Kristallografiya,* **37**, 598.

Brydson, R., Garvie, L. A. J., Craven, A. J., Sauer, H., Hofer, F., and Cressey, G., 1993, *J. Phys.: condens. Matter,* **5**, 9379.

Brydson, R., Sauer, H., Engel, W., and Hofer, F., 1992, *J. Phys.: condens. Matter,* **4**, 3429.

Brydson, R., Sauer, H., Engel, W., Thomas, J. M., Zeitler, E., Kosugi, N., and Kuroda, H., 1989, *J. Phys.: condens. Matter,* **1**, 797.

Bursill, L. A., and Grzinic, G., 1980, *Acta crystallogr.* B, **36**, 2902.

Cheary, R. W., 1990, *Acta crystallogr.* B, **46**, 599.

Cheary, R. W., and Squadrito, R., 1989, *Acta crystallogr.* B, **45**, 205.

Cheary, R. W., Thompson, R., and Watson, P., 1996, *Mater. Sci. Forum,* **228–231**, 777.

Cohen, R. E., and Krakauer, H., 1990, *Phys. Rev.* B, **42**, 6416.

Crocombette, J. P., and Jollet, F., 1994, *J. Phys.: condens. Matter,* **6**, 10 811.

de Groot, F. M. F., Figueirdo, M. O., Basto, M. J., Abbate, M., Petersen, H., and Fuggle, J. C., 1992, *Phys. Chem. Miner.,* **19**, 140.

Egerton, R. F., 1996, *Electron Energy-Loss Spectroscopy in the Electron Microscope* (New York: Plenum).

Fanchon, E., Vicat, J., Hodeau, J. L., Wolfers, P., Qui, D. T., and Strobel, P., 1987, *Acta Crystallogr.* B, **43**, 440.

Fink, J., Müller-Heinzerling, T., Scheerer, B., Speier, W., Hillebrecht, F. U., Fuggle, J. C., Zaanen, J., and Sawatzky, G. A., 1985, *Phys. Rev.* B, **32**, 4899.

Guerlin, T., 1996, Ph.D. thesis, Free University of Berlin.

Higuchi, T., Tsukamoto, T., Watanabe, M., Grush, M. M., Callcott, T. A., Perera, R. C., Ederer, D. L., Tokura, Y., Harada, Y., Tezuka, Y., and Shin, S., 1999, *Phys. Rev.* B, **60**, 7711.

Höche, T., Kleebe, H.-J., and Brydson, R., 2001, *Phil. Mag.* A, **81**, 825.

Langenhorst, F., and van Aken, P. A., 2000, *Bull. Liaison SFMC,* **12**, 29.

Leapman, R. D., Grunes, L. A., and Fejes, P. L., 1982, *Phys. Rev.* B, **26**, 614.

Lusvardi, V. S., Barteau, M. A., Chen, J. G., Eng, J., Frühberger, B., and Teplyakov, A., 1998, *Surf. Sci.,* **397**, 237.

Möhr, S., and Müller-Buschbaum, H., 1993, *J. Alloys Compounds,* **199**, 203.

Morikawa, K., Mizokawa, T., Fujimori, A., Taguchi, Y., and Tokura, Y., 1996, *Phys. Rev.* B, **54**, 8446.

Otten, M. T., Miner, B., Rask, J. H., and Buseck, P. R., 1985, *Ultramicroscopy*, **18**, 285.

Perez-Mato, J. M., Zakhour-Nakhl, M., Darriet, J., and Elcoro, L., 2001, *Ferroelectrics,* **250**, 13.

Rose, H., 1999, *Ultramicroscopy,* **78**, 13.

Rosshirt, E., Frey, F., and Boysen, H., 1991, *Neues Jb Miner. Abh.,* **163**, 101.

Rosshirt, E., Frey, F., Kupcik, V., and Miehe, G., 1990, *J. appl. Crystallogr.,* **23**, 21.

Ruus, R., Kikas, A., Saar, A., Ausmees, A., Nommiste, E., Aarik, J., Aidla, A., Uustare, T., and Martinson, I., 1997, *Solid St. Commun.,* **104**, 199.

SCHMACHTEL, J., and MÜLLER-BUSCHBAUM, H., 1977, *Z. anorg. allg. Chem.,* **435**, 243; 1980, *Z. Naturf.* (b), **35**, 332.
SCHNEIDER, R., WOLTERSDORF, J., and LICHTENBERGER, O., 1996, *J. Microsc. (London)*, **183**, 39.
VAN AKEN, P. A., and LIEBSCHER, B., 2002, *Phys. Chem. Miner.,* **29**, 188.
VAN AKEN, P. A., LIEBSCHER, B., and STYRSA, V. J., 1998, *Phys. Chem. Miner.,* **25**, 323.
WEBER, H. P., and SCHULZ, H., 1983, *Solid St. Ionics,* **9–10**, 1337.
YOSHIYA, M., TANAKA, I., KANEKO, K., and ADACHI, H., 1999, *J. Phys.: condens. Matter,* **11**, 3217.